Neuroanatomical substrates of generalized brain dysfunction in COVID-19

Virginia Newcombe,[1,2] Lennart Spindler,[1,3] Tilak Das,[4] Stefan Winzeck,[1,5] Kieren Allinson,[6] Emmanuel Stamatakis,[1,2,3] David Menon[1,2] on behalf of the Cambridge NeuroCovid Imaging Collaborators.

Affiliations

1. Division of Anaesthesia, Department of Medicine, University of Cambridge
2. Wolfson Brain Imaging Centre, University of Cambridge
3. Department of Clinical Neurosciences, University of Cambridge
4. Department of Radiology, Cambridge University Hospitals NHS Foundation Trust
5. BioMedIA group, Department of Computing, Imperial College, London
6. Addenbrooke's Hospital, Department of Pathology, Cambridge, UK

*Authors for correspondence:

Virginia FJ Newcombe: vfjn2@cam.ac.uk; Box 93, Addenbrooke's Hospital, Cambridge CB2 2QQ, UK

David K Menon: dkm13@cam.ac.uk; Box 93, Addenbrooke's Hospital, Cambridge CB2 2QQ, UK

Cambridge NeuroCovid Imaging Collaborators:

Fahim Anwar, Edward Bullmore, Alasdair Coles, Jonathan Coles, Tilak Das, Joanne Jones, Victoria Lupson,

David Menon, Edward Needham, Virginia Newcombe, James Rowe, Stephen Sawcer, Lennart Spindler,

Emmanuel Stamatakis, Fernanda Valerio.

Dear Editor,

Central nervous system involvement is common in COVID-19, and may be driven by many mechanisms [1]. Reports of brain magnetic resonance imaging (MRI) findings in individual patients or small case series have generally focused on discrete pathologies such as stroke or focal abnormalities. However, these reports do not elucidate more generalized abnormalities of central nervous function, such as the alteration of mental status in a third of patients [2], or quantitative imaging correlates of reported brainstem pathology [3].

We report MRI findings in six patients with severe COVID-19 related respiratory failure (WHO Ordinal Scale 7), imaged 19 days (range 16-26) post-admission, using conventional MRI and diffusion tensor imaging (DTI, Supplemental Table 1). The scans were performed for clinical reasons while the patients were in the intensive care unit with data prospectively collected; persistent unresponsiveness after washout of sedative agents (n=4); severe delirium (n =1); or generalised myoclonus (n=1). Three patients had small acute ischemic lesions in the frontal deep white matter and two of these also had subarachnoid, intraventricular, or small parenchymal hemorrhage. However, none of the patients had abnormalities on conventional MRI that explained their clinical presentation or indicated hypoxic-ischemic injury.

DTI characterises the diffusion of water molecules in tissue environments which are influenced by the microstructural organization of tissues. The diffusion tensor can be used to represent the magnitude of water diffusion (quantified as mean diffusivity (MD), which quantifies overall diffusion of water in tissue compartments), describe whether such diffusion is directionally non-uniform (fractional anisotropy, which classically changes with white matter pathology), and characterize the orientation of that direction (eigenvectors/eigenvalues, used for tractography; a modelling technique used to map out white matter tracts, see Supplementary Tables 3, 4 and 5 for tract names).

All of the COVID-19 patients showed pervasive abnormalities on quantitative DTI compared to controls (Figure 1, Supplemental Tables 2-5), with increased mean diffusivity (MD) in frontal, temporal, parietal, and occipital cortices and hippocampi, consistent with vasogenic edema. In contrast, the mesencephalic and pontine reticular formations showed significant MD reductions, suggesting cytotoxic edema. No significant differences were seen in the basal ganglia or thalami. COVID-19 patients had significantly lower fractional anisotropy in several white matter tracts (Figure 1B), suggesting microstructural disruption (eg edema, inflammation). All reported differences remained significant after stringent correction for multiple comparisons ($p < 0.05$, Bonferroni corrected).

These findings suggest pervasive vasogenic edema in cortical grey and white matter tracts, recapitulating postmortem findings in sepsis-associated encephalopathy [4]. The presence of edema in brainstem regions, however, requires alternate explanation. The mesencephalic and pontine reticular formations are key glutamatergic nuclei, suggesting possible excitotoxic injury. Alternatively, restricted diffusion may arise from inflammatory cell infiltration, as described in other viral encephalitides [5]. Such brainstem involvement may reflect direct SARS-CoV-2 infection, perhaps entering the brain through cranial nerves [1].

One patient (Patient 2, Supplementary Table 1) underwent a post-mortem examination. There was no evidence of established hypoxic-ischaemic brain injury and no vascular micro-thrombi were seen. In the dorsal medulla, there was a moderate parenchymal infiltrate of T-lymphocytes ($CD3^+CD8^+$), and activated microglia ($CD68^+$) involving the motor nucleus of the vagus nerve, nucleus ambiguus, solitary tract nucleus and inferior cerebellar peduncle (Figure 2). The inflammatory infiltrate did not involve ventral medullary structures such as the pyramidal tracts or olivary nuclear complexes. A mild perivascular infiltrate of T-lymphocytes ($CD3^+CD8^+$) was found in the cerebral and cerebellar leptomeninges, cerebral white matter, and basal ganglia. Both ISH and RT-PCR for SARS-CoV-2 RNA were negative in paraffin-embedded tissue sampled from the area of encephalitis in the medulla.

These novel findings are important for three reasons. First, we show that quantitative DTI may be abnormal in brain tissue that appears radiologically normal. Second, the widespread cortical and hippocampal abnormalities may explain mental status alterations seen in many patients. Finally, abnormalities in key brainstem arousal nuclei provide plausible neuroanatomical substrates for alteration of the sensorium in our patients. Further work is needed to ascertain whether these features reflect generic sepsis related encephalopathy or are specific to SARS-CoV-2.

Author contributions

VFJN and DKM designed the study. VFJN, LRBS, SW and EAS analysed the data. TD provided neuroradiology input. KA provided neuropathology input. All authors interpreted the data and contributed to the writing of the letter.

Compliance with ethical standards

The Local Research Committee approved the use of the data used in this study (NIHR BioResource REC reference; 17/EE/0025, IRAS project ID 220277). Assent was obtained from next of kin. For control data ethical approval was obtained from the Local Research Ethics Committee (LREC 97/290 and 17/EE/0032, IRAS project ID 204052) and written consent was obtained.

Conflicts of Interest

All the authors declare no conflict of interest

References

1. Zubair AS, McAlpine LS, Gardin T, Farhadian S, Kuruvilla DE, Spudich S. Neuropathogenesis and Neurologic Manifestations of the Coronaviruses in the Age of Coronavirus Disease 2019: A Review [published online ahead of print, 2020 May 29]. JAMA Neurol. 2020;10.1001/jamaneurol.2020.2065.
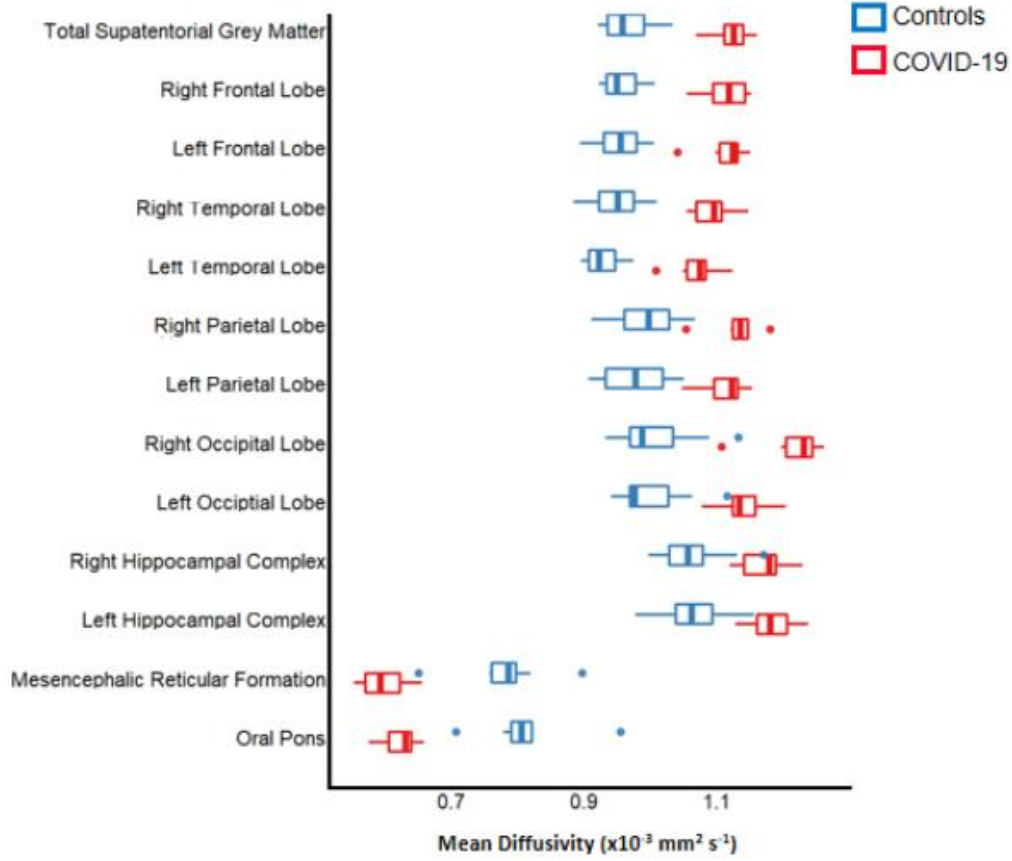
2. Varatharaj A, Thomas N, Ellul M, et al; On Behalf of the CoroNerve Studies Group. UK-wide surveillance of neurological and neuropsychiatric complications of COVID-19: The first 153 patients. Lancet Psychiatry 2020;S2215-0366(20)2-287-X.

3. Sharshar T, Gray F, Poron F, Raphael JC, Gajdos P, Annane D. Multifocal necrotizing leukoencephalopathy in septic shock. Crit Care Med 2002; **30**(10):2371-2375.

4. von Weyhern CH, Kaufmann I, Neff F, Kremer M. Early evidence of pronounced brain involvement in fatal COVID-19 outcomes [published online ahead of print, 2020 Jun 4]. Lancet. 2020; S0140-6736(20)31282-4. doi:10.1016/S0140-6736(20)31282-4

5. Koeller KK, Shih RY. Viral and Prion Infections of the Central Nervous System: Radiologic-Pathologic Correlation: From the Radiologic Pathology Archives. Radiographics 2017; **37**:199-233
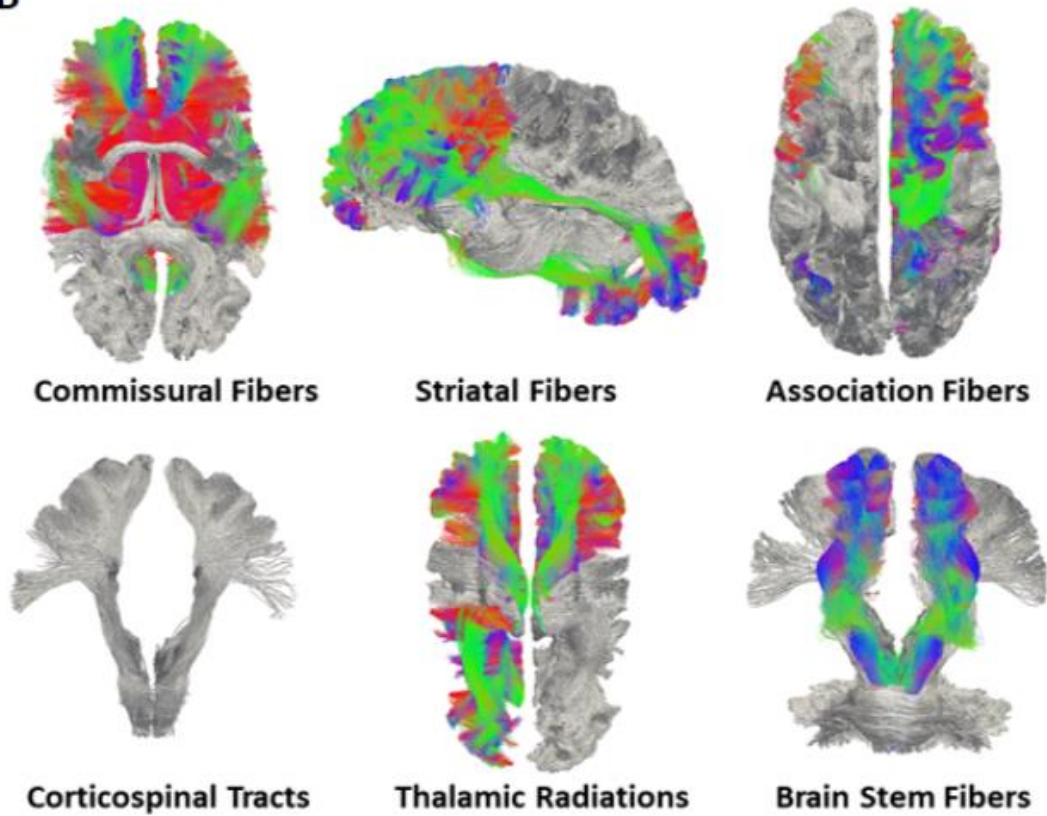
Legend to Figures:

Figure 1. Panel A shows boxplots of mean diffusivity (MD) in gray matter regions where COVID-19 patients show significant differences compared to age- and sex-matched control subjects. Panel B shows the group wise comparison of parcellated white matter tracts. Tracts in colour (not grey) have significantly lower fractional anisotropy (FA) in the COVID-19 cases when compared to age and sex-matched controls. The colour coding reflects directionality of fibres, with green denoting anterior/posterior, blue superior/inferior, and red right/left directionality.

Figure 2. Histology of the dorsal medulla (patient 2). Panel A: CD3 (x200 magnification) immunohistochemistry showing a moderate parenchymal infiltrate of T-cells. Panel B: CD68 immunohistochemistry showing micogliosis with microglial nodules.

A
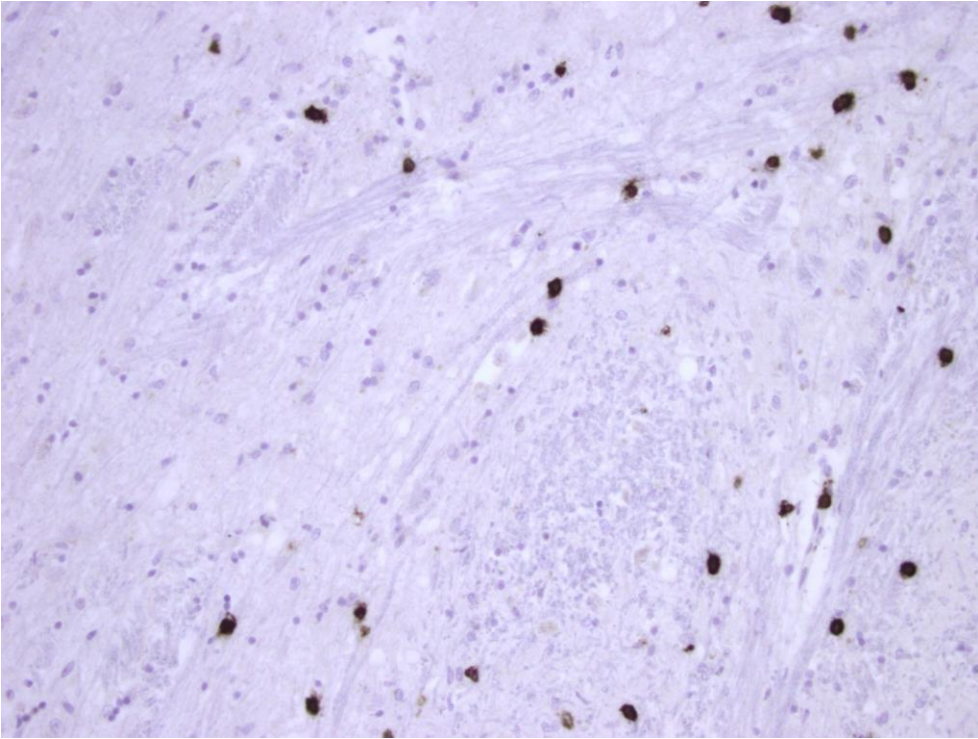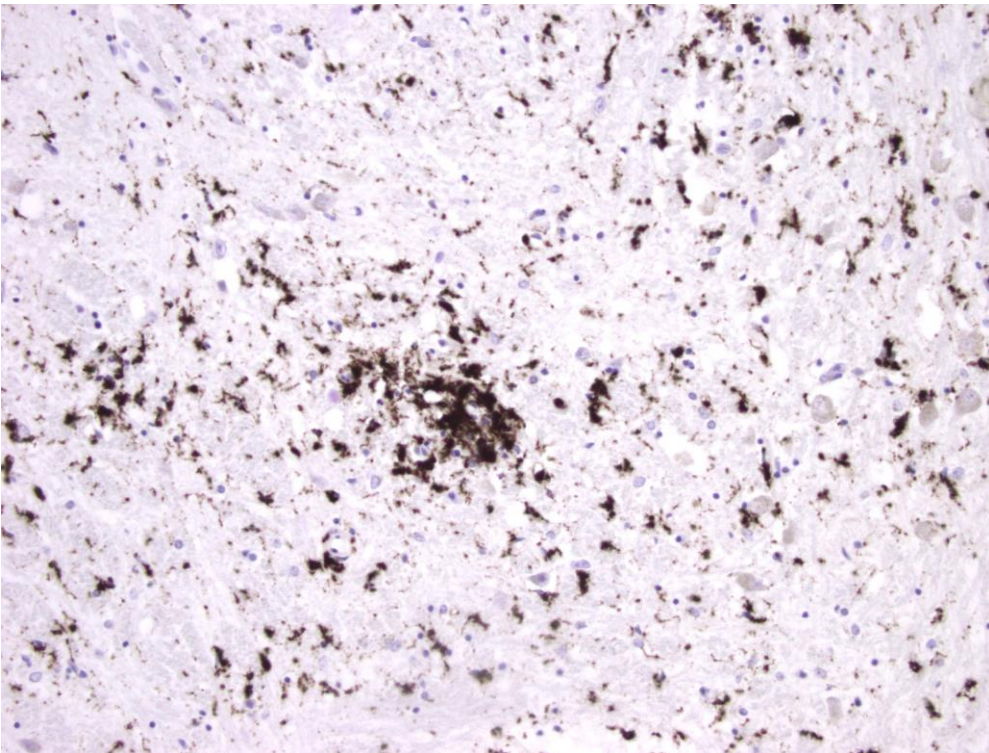

Mean Diffusivity ($\times 10^{-3}$ mm^2 s^{-1})

B

Commissural Fibers

Striatal Fibers

Association Fibers

Corticospinal Tracts

Thalamic Radiations

Brain Stem Fibers

A

B

Supplementary Material

Table of Contents

Supplementary Methods

Imaging Methods

Control Data Collection

Fifteen controls (10 male, age range 45 to 77) were selected to match for age and gender from healthy volunteers collected pre-pandemic as part of traumatic brain injury and dementia studies performed at the Wolfson Brain Imaging Center (WBIC) using the exact same sequences. There were no scanner upgrades between control and patient data collection.

MRI Imaging and Image Analysis

MRI was performed in the Wolfson Brain Imaging Centre (WBIC) while the patients were intubated and ventilated on the 3 Tesla MAGNETOM Prisma Siemens scanner. All patients were sedated with fentanyl (2-6 mcg/kg/h), in combination with propofol (2-4 mg/kg/h) and/or midazolam (0.1-0.2 mg/kg/h), and received bolus doses of rocuronium (0.1 mg/kg) to facilitate mechanical ventilation and ensure immobility during the scan. Clinical details can be seen in Table 1.

Sequences included volumetric T1-weighted MPRAGE (voxel size 1mm), volumetric fluid attenuated inversion recovery (FLAIR), T2-weighted Turbo spin echo, susceptibility weighted imaging (SWI) or T2*-weighted Gradient Recalled Echo, and diffusion tensor imaging (DTI). The DTI parameters were 2mm isotropic voxels, 63 non-collinear directions and b-value of 1000 s/mm^2, matrix size 192x192x126, repetition time = 7800ms, echo time = 90ms. Clinical sequences were reported by a qualified neuroradiologist.

After neck-cropping and correcting for scanner field inhomogeneities, brain parcellation was performed on the T1-weighted images, using MALP-EM (Multi-Atlas Label Propagation with Expectation-Maximisation based refinement) which provides robust segmentation of the grey matter even when anatomy is distorted due to trauma [1]. The 138 anatomical regions were collapsed into 20 grey matter regions of interest (ROIs) (Table 2).

All DTI data were corrected for noise [2,3], Gibb's ringing artefacts [4], head motion, and eddy current artefacts [5] and inhomogeneities in the magnetic field [6]. Diffusion tensors were fitted via weighted least squares to derive mean diffusivity (MD) and fractional anisotropy (FA) maps using FSL (https://fsl.fmrib.ox.ac.uk/). White matter parcellation into 72 tracts was performed using TractSeg, a convolutional neural network based approach [7].

In order to analyse brainstem regions in greater detail, FA and MD images were non-linearly projected to the Montreal Neurological Institute (MNI) atlas space. For this, FA maps were first rigidly co-registered to the corresponding T1 weighted image and the same transformation was applied to align MD maps. T1 weighted images were spatially normalised to MNI space via SPM12 statistical parametric mapping (SPM- https://www.fil.ion.ucl.ac.uk/spm/). Found transformation parameters were then applied to the co-registered diffusion parameter maps (i.e. FA and MD). To facilitate ROI value extractions, two dummy linear regression models (one with all spatially normalised FA and another with all spatially normalised MD images) were constructed using SPM12, a brain image analysis toolbox written for Matlab (https://uk.mathworks.com/products/matlab.html). Principal eigenvectors were extracted for each ROI from the spatially normalised FA and MD images. In other words, a summary of the values within an ROI was extracted, which unlike the average, does not assume homogenous responses within the ROI [8]. The three large brainstem ROIs i.e. midbrain, pons and medulla were constructed using the Matlab based WFU PickAtlas toolbox (https://www.nitrc.org/projects/wfu_pickatlas) [9]. Gray matter (GM) and white matter (WM) volumes for the midbrain, pons and medulla were obtained by masking those ROIs with thresholded GM and WM SPM12 priors.

Smaller brainstem ROIs (dorsal raphe, mesencephalic reticular formation, periaqueductal grey matter, and pontine reticular formation) were obtained using the Harvard Ascending Arousal Network Atlas, which comprises a physiologically relevant set of Brainstem ROIs of the ascending reticular activating system of the brainstem [10,11]. The faithful co-registration of these ROIs to our

anatomical scans and FA/MD images was extensively assessed visually. In order to prevent the risk of mis-registration in small ROIs, we only measured DTI metrics in regions from this atlas which comprised at least 250 voxels (0.25 ml).

All raw data and pipeline outputs were visually inspected, and motion parameters for DTI calculated. No subjects needed to be excluded from the analysis due to excessive head motion or other artefact. Regional volumes, mean FA and mean MD values were obtained for the grey and white matter parcellations.

For visualisation of significant MD differences, the CONN Toolbox standard template was used (https://web.conn-toolbox.org), and for FA tracts an exemplar subject (898176) was used from the Human Connectome Project. The segmented dataset is available at https://zenodo.org/record/1477956#.Xt5BJTOSlZc.

Post-mortem Methods

A detailed autopsy was performed on patient B after a post mortem interval of nine days. The brain was removed and fixed in 20% neutral buffered formalin for four weeks prior to dissection. Histological blocks included medulla, pons, midbrain, cerebellum, basal ganglia, thalamus and frontal, temporal, parietal and occipital lobes. These were embedded in paraffin wax from which 10micron sections were cut and mounted on glass slides. Slides were examined with haematoxylin and eosin (H&E) stains and immunohistochemistry for CD3, CD8, CD4 (all Leica) and CD68 (Dako) was performed using the Leica Bond-Max III system. RNAscope® in situ hybridisation (ISH) using the V-nCoV2019-S probe and RT-PCR SARS-CoV-2 ribonucleic acid (RNA) was performed in paraffin-embedded brain tissue sampled from areas of pathology, with comparison to suitable controls.

Statistical Analysis

Data were analysed in R version 3.6.0. Results are reported as Median [Interquartile range]. Comparison between groups was performed using a Mann-Whitney U Test (Wilcoxon rank sum test) with both unadjusted p-values and adjusted p-values using a Bonferroni test for each analysis. Statistical significance was determined using a Bonferroni test threshold of 5%.

Supplementary Tables: The following supplementary tables provide comparisons of DTI metrics between the cohort of COVID-19 patients and age and sex-matched healthy controls. Asterisks (*) indicate statistical comparisons that survive Bonferroni correction for multiple comparisons, which are also highlighted in **bold** text**.** We also compared the volumes of each of the ROIs that we report on. However, following correction for multiple comparisons, we found no significant differences between patients with COVID-19 and the control group for the volume of any ROI. Consequently, these data are not shown, but are available upon request. Please see the referenced open access review for further details about DTI, the interpretation of metrics and in its use in neurological diseases [12].

Table 1: Subject characteristics

Patient	1	2	3	4	5	6
Age (years)	71	67	71	74	74	48
Sex	M	M	F	M	M	M
Symptom onset to imaging (days)	40	Uncertain (secondary transfer)	31	26	14	29
Admission to imaging (days)	19	18	22	19	16	27
Covid-19 severity (WHO Ordinal Scale)	7	7	7	7	7	7
Chest imaging findings	Bilateral patchy ground glass foci both lungs, bilateral pleural effusions.	Bilateral ground glass changes and dense bi-basal consolidation, left sided pleural effusion.	Bilateral ground glass changes, right upper lobe consolidation, Left sided effusion. Right lower lobe pulmonary embolism (PE)	Bilateral ground glass opacity and consolidation.	Bilateral lower lobe ground glass opacity and consolidation.	Right lower lobe consolidation.
PaO2/FIO2 (mmHg) at time of imaging	114	323	160	207	200	213
SOFA Score on day of imaging	8	9	11	10	11	9
Renal replacement required	No	Yes	Yes	Yes	Yes	Yes
Cardiac Arrest	No	No	No	No	No	No
Confirmed period of hypoxia	No	No	Yes – PE with ~60 minutes of saturations in 60s	No	No	No
SARS-CoV-2 PCR Ct	18	Positive, but Ct unavailable (secondary transfer)	20	Positive, but Ct unavailable (secondary transfer)	25	15
Lowest lymphocyte count (x10^9/L)	0.35	0.44	0.30	0.74	0.87	0.30
CRP (mg/L)	367	300	450	443	258	450
PCT (ng/ml)	11	0.85	0.94	2.5	9.08	2.0
Ferritin (µg/L)	4000	9000	755	1400	6915	755
D-dimer (µg/ml)	952	4035	3473	5374	2764	2543
IL-6 (pg/ml)	54.1	N/A	N/A	49.9	124.5	16.6
PT (seconds)	15.2	12.0	13.1	11.8	12.2	
aPTT (seconds)	30.9	28.5	65.3	33.5	51.1	40.1
Fibrinogen (g/L)	6.16	5.67	7.19	8.26	5.67	4.47
Platelet count (x10^9/L)	427	400	300	208	355	436

6

Table 1: Subject characteristics (continued)

Patient	1	2	3	4	5	6
Indication for imaging	Generalised myoclonus, level of consciousness not assessable	Failure to regain consciousness after stopping sedation	Failure to regain consciousness after stopping sedation; facial myoclonus	Failure to regain consciousness after stopping sedation	Failure to regain consciousness after stopping sedation	Persistent agitation, concern about pituitary axis dysfunction and severe delirium preventing ventilatory weaning
Days off sedation at time of imaging	Still sedated	8	3	5	8	Sedation to control agitation
At time of imaging:						
Pupillary light reflex	Equal and reactive	Equal and reactive	Equal and reactive	Equal and reactive	Equal and reactive	Equal and reactive
Corneal reflex	Present	Present	Present	Present	Present	Present
Eye movements	Saccadic intrusions and episodes of convergence	No abnormality notedrecorded	No abnormality notedrecorded	No abnormality notedrecorded	No abnormality notedrecorded	No abnormality notedrecorded
Cough reflex	Present	Present	Present	Present	Absent	Present
At time of imaging:						
RASS	-3 to -4	-3	-3	-3	-4	-1 to +1 (while sedated)
GCS	E1 M2 Vt	E1 M2 Vt	E4 M1 Vt	E2 M1 Vt	E2 M1 Vt	E4 M5 Vt when not sedated
MRI imaging findings (Conventional Sequences)	No focal abnormality	Small foci of SDH right cerebellum, SAH in cerebellar sulci. Small SDH at the foramen magnum. IVH in occipital horns. Subcortical focus of restricted diffusion in the pre-central gyrus and right frontal deep white matter.	Non-specific supratentorial WMH	Non-specific supratentorial WMH. Focus of possible restricted diffusion right frontal deep white matter	Peripheral microhaemorrhages (?CAA), old R basal ganglia bleed (likely hypertensive), left superior frontal sulcal SAH, L frontal acute ischaemic focus. Tiny left occipital horn IVH.	No focal abnormality
Current status	Alive, undergoing neurorehabilitation	Dead – multi-organ failure	Dead – multi-organ failureDead	Alive, undergoing neurorehabilitation	Dead – multi-organ failureDead	Alive, undergoing neurorehabilitation

PE: Pulmonary Embolism; **SOFA:** Sequential Organ Failure Assessment; **Ct:** Cycle threshold value; **CRP:** C-reactive protein; **PCT:** procalcitonin; **IL-6:** Interleukin-6; **PT:** Prothrombin time; **APTT:** Activated Partial Thronboplastin Time; **CAM-ICU:** Confusion Assessment method for the ICU; **RASS**: Richmond Agitation-Sedation Scale; **GCS**: Glasgow Coma Score

Table 2. Mean diffusivity (MD; quantifies overall diffusion of water in tissue compartments) and fractional anisotropy (FA; a measure of directionality of diffusion) for grey matter regions. All data reported as median (IQR).

	Mean Diffusivity (x10^{-3} mm^2/s)				Fractional Anisotropy			
	Controls	COVID-19	p-value	Adjusted p-value	Controls	COVID-19	p-value	Adjusted p-value
Supratentorial	0.96 (0.91-1.02)	1.10 (1.07-1.13)	<0.001	**0.003***	0.14 (0.13-0.15)	0.14 (0.13-0.14)	0.07	1.00
Right Frontal Lobe	0.95 (0.91-0.99)	1.11 (1.05-1.15)	<0.001	**0.003***	0.15 (0.14-0.16)	0.15 (0.14-0.16)	0.89	1.00
Left Frontal Lobe	0.96 (0.91-1.01)	1.10 (1.07-1.13)	<0.001	**0.003***	0.15 (0.14-0.16)	0.14 (0.13-0.15)	0.25	1.00
Right Temporal Lobe	0.95 (0.90-1.00)	1.10 (1.06-1.14)	<0.001	**0.003***	0.14 (0.13-0.15)	0.14 (0.13-0.15)	0.34	1.00
Left Temporal Lobe	0.92 (0.88-0.96)	1.10 (1.07-1.13)	<0.001	**0.003***	0.15 (0.14-0.16)	0.14 (0.13-0.15)	0.21	1.00
Right Parietal Lobe	1.00 (0.93-1.07)	1.10 (1.08-1.12)	<0.001	**0.006***	0.13 (0.12-0.14)	0.13 (0.12-0.14)	0.89	1.00
Left Parietal Lobe	0.98 (0.89-1.07)	1.09 (1.06-1.14)	<0.001	**0.01***	0.14 (0.13-0.15)	0.14 (0.13-0.15)	0.75	1.00
Right Hippocampus	1.10 (1.05-1.15)	1.20 (1.15-1.25)	0.001	**0.03***	0.16 (0.14-0.18)	0.14 (0.13-0.15)	0.03	0.86
Left Hippocampus	1.10 (1.05-1.16)	1.20 (1.16-1.25)	<0.001	**0.006***	0.16 (0.15-0.18)	0.16 (0.15-0.17)	0.10	1.00
Right Occipital Lobe	0.99 (0.92-1.06)	1.20 (1.16-1.24)	<0.001	**0.006***	0.12 (0.11-0.13)	0.11 (0.10-0.12)	0.03	0.86
Left Occipital Lobe	0.98 (0.92-1.04)	1.10 (1.07-1.13)	<0.001	**0.006***	0.13 (0.12-0.14)	0.12 (0.11-0.13)	0.10	1.00
Right Thalamus	0.83 (0.81-0.85)	0.90 (0.88-0.92)	0.002	0.06	0.34 (0.32-0.36)	0.32 (0.29-0.35)	0.02	0.66
Left Thalamus	0.81 (0.79-0.83)	0.89 (0.85-0.93)	0.003	0.09	0.35 (0.34-0.36)	0.32 (0.30-0.34)	0.01	0.36
Right Globus Pallidus	0.72 (0.69-0.75)	0.74 (0.64-0.84)	0.10	1.00	0.28 (0.23-0.33)	0.28 (0.24-0.32)	0.44	1.00
Left Globus Pallidus	0.67 (0.61-0.73)	0.68 (0.60-0.76)	0.75	1.00	0.34 (0.30-0.38)	0.32 (0.29-0.35)	0.29	1.00
Right Putamen	0.72 (0.70-0.74)	0.77 (0.69-0.85)	0.002	0.06	0.23 (0.22-0.25)	0.25 (0.22-0.29)	0.62	1.00
Left Putamen	0.68 (0.64-0.73)	0.73 (0.61-0.85)	0.04	1.00	0.27 (0.23-0.31)	0.27 (0.21-0.33)	1.00	1.00
Right Caudate	0.94 (0.84-1.04)	1.00 (0.76-1.24)	0.18	1.00	0.20 (0.18-0.22)	0.21 (0.18-0.24)	0.55	1.00
Left Caudate	0.95 (0.89-1.01)	1.00 (0.86-1.14)	0.18	1.00	0.20 (0.18-0.22)	0.23 (0.21-0.26)	0.15	1.00
Cerebellar	0.99 (0.92-1.06)	1.20 (1.17-1.23)	0.007	0.19	0.16 (0.15-0.17)	0.15 (0.14-0.16)	0.10	1.00
Midbrain	1.40 (1.17-1.63)	1.40 (1.07-1.73)	0.34	1.00	0.33 (0.30-0.37)	0.32 (0.28-0.37)	0.68	1.00
Pons	1.40 (1.20-1.60)	1.10 (1.03-1.18)	0.003	0.09	0.31 (0.29-0.33)	0.31 (0.30-0.32)	0.49	1.00
Medulla	0.90 (0.80-1.00)	0.90 (0.83-0.98)	0.13	1.00	0.29 (0.25-0.33)	0.30 (0.25-0.35)	0.29	1.00
Dorsal Raphe	1.30 (1.00-1.60)	0.90 (0.60-1.2)	0.007	0.19	0.44 (0.34-0.54)	0.48 (0.44-0.52)	0.12	1.00
Mesencephalic reticular formation	0.79 (0.75-0.83)	0.59 (0.54-0.64)	<0.001	**0.006***	0.31 (0.25-0.37)	0.38 (0.32-0.44)	0.002	0.06
Periaqueductal	1.30 (1.15-1.45)	0.95 (0.70-1.20)	0.002	0.05	0.21 (0.16-0.26)	0.30 (0.17-0.43)	0.02	0.49
Pontine reticular formation	0.81 (0.78-0.84)	0.63 (0.60-0.67)	<0.001	**0.003***	0.55 (0.51-0.59)	0.52 (0.47-0.57)	0.49	1.00

8

Table 3. Mean diffusivity and fractional anisotropy for the projection fibre tracts, commissural fibre tracts and thalamic radiations. All data reported as median (IQR).

	Mean Diffusivity ($\times10^{-3}$ mm^2/s)				Fractional Anisotropy			
	Controls	COVID-19	P-value	Adjusted P-Value	Controls	COVID-19	P-value	Adjusted P-Value
Projection Fibres								
Corticospinal tract Left	0.71 (0.68-0.74)	0.73 (0.63-0.83)	0.29	1.00	0.50 (0.47-0.53)	0.47 (0.45-0.49)	0.02	1.00
Corticospinal tract Right	0.71 (0.68-0.74)	0.74 (0.67-0.81)	0.22	1.00	0.50 (0.48-0.52)	0.46 (0.41-0.51)	0.002	0.13
Commissural Fibres								
CC Genu	0.79 (0.75-0.83)	0.91 (0.86-0.96)	<0.001	**0.007***	0.40 (0.36-0.44)	0.33 (0.32-0.34)	<0.001	**0.007***
CC Body	0.77 (0.73-0.81)	0.83 (0.76-0.90)	<0.001	0.05	0.44 (0.40-0.48)	0.39 (0.38-0.40)	<0.001	**0.03***
Splenium	0.83 (0.80-0.86)	0.95 (0.88-1.02)	<0.001	0.05	0.39 (0.37-0.41)	0.34 (0.30-0.38)	0.002	0.14
Commissure Anterior	0.81 (0.78-0.84)	0.90 (0.81-0.99)	0.001	0.08	0.40 (0.38-0.42)	0.35 (0.33-0.37)	0.04	1.00
Fornix left	1.40 (1.20-1.60)	1.70 (1.49-1.91)	0.10	1.00	0.42 (0.40-0.44)	0.34 (0.22-0.46)	0.22	1.00
Fornix right	1.50 (1.21-1.79)	1.6 (1.31-1.89)	0.73	1.00	0.40 (0.36-0.44)	0.37 (0.28-0.46)	0.66	1.00
Thalamic Radiations								
Thalamo-prefrontal Left	0.75 (0.70-0.80)	0.83 (0.74-0.92)	0.001	0.09	0.39 (0.37-0.42)	0.35 (0.33-0.37)	<0.001	**0.007***
Thalamo-prefrontal Right	0.75 (0.72-0.79)	0.85 (0.78-0.92)	<0.001	**0.007***	0.38 (0.36-0.40)	0.33 (0.31-0.35)	<0.001	**0.007***
Thalamo-premotor Left	0.72 (0.68-0.76)	0.78 (0.67-0.89)	0.002	0.13	0.42 (0.40-0.44)	0.38 (0.34-0.42)	<0.001	**0.02***
Thalamo-premotor Right	0.71 (0.68-0.74)	0.78 (0.66-0.90)	0.001	0.08	0.43 (0.41-0.45)	0.38 (0.33-0.43)	<0.001	**0.01***
Thalamo-precentral Left	0.71 (0.69-0.73)	0.74 (0.64-0.84)	0.01	0.97	0.45 (0.43-0.47)	0.40 (0.38-0.43)	0.005	0.32
Thalamo-precentral Right	0.71 (0.68-0.74)	0.74 (0.66-0.82)	0.03	1.00	0.44 (0.43-0.45)	0.40 (0.35-0.45)	0.001	0.08
Thalamo-postcentral Left	0.71 (0.68-0.74)	0.76 (0.73-0.79)	<0.001	**0.03***	0.45 (0.43-0.48)	0.40 (0.36-0.44)	0.002	0.14
Thalamo-postcentral Right	0.71 (0.68-0.74)	0.77 (0.75-0.79)	<0.001	**0.02***	0.45 (0.43-0.47)	0.41 (0.39-0.43)	0.005	0.32
Thalamo-parietal Left	0.76 (0.72-0.80)	0.84 (0.82-0.86)	<0.001	**0.007***	0.41 (0.38-0.44)	0.38 (0.36-0.40)	<0.001	0.051
Thalamo-parietal Right	0.77 (0.73-0.81)	0.84 (0.81-0.87)	<0.001	**0.007***	0.40 (0.37-0.43)	0.37 (0.36-0.38)	<0.001	**0.01**
Thalamo-occipital Left	0.81 (0.78-0.84)	0.91 (0.85-0.97)	0.001	0.09	0.36 (0.33-0.39)	0.33 (0.32-0.34)	<0.001	0.051
Thalamo-occipital Right	0.80 (0.77-0.83)	0.93 (0.88-0.98)	0.000	**0.01***	0.38 (0.37-0.39)	0.33 (0.31-0.35)	<0.001	**0.01***
Superior Thalamic Radiation Left	0.69 (0.67-0.71)	0.72 (0.65-0.79)	0.002	0.13	0.47 (0.45-0.49)	0.43 (0.40-0.46)	0.03	1.00
Superior Thalamic Radiation Right	0.70 (0.68-0.72)	0.72 (0.65-0.79)	0.005	0.32	0.45 (0.44-0.47)	0.43 (0.42-0.440	0.002	0.13
Anterior Thalamic Radiation Left	0.77 (0.72-0.82)	0.86 (0.78-0.94)	<0.001	**0.03***	0.37 (0.35-0.39)	0.32 (0.30-0.34)	<0.001	**0.007***
Anterior Thalamic Radiation Right	0.76 (0.73-0.79)	0.88 (0.82-0.94)	0.01	0.72	0.37 (0.35-0.39)	0.31 (0.29-0.33)	<0.001	**0.01***

Table 4. Mean diffusivity and fractional anisotropy for the striatal fibre tracts and brainstem tracts. All data reported as median (IQR).

	Mean Diffusivity (x10⁻³ mm²/s)				Fractional Anisotropy			
	Controls	COVID-19	P-value	Adjusted P-Value	Controls	COVID-19	P-value	Adjusted P-Value
Striatal Fibres								
Striato-fronto-orbital Left	0.77 (0.74-0.80)	0.89 (0.83-0.95)	<0.001	**0.04***	0.39 (0.35-0.43)	0.33 (0.31-0.35)	<0.001	**0.01***
Striato-fronto-orbital Right	0.75 (0.71-0.80)	0.87 (0.81-0.93)	<0.0018	**0.04***	0.40 (0.37-0.44)	0.33 (0.32-0.34)	0.001	0.08
Striato-prefrontal Left	0.76 (0.71-0.81)	0.84 (0.75-0.93)	<0.001	0.051	0.38 (0.35-0.41)	0.33 (0.31-0.35)	<0.001	**0.007***
Striato-prefrontal Right	0.75 (0.71-0.79)	0.85 (0.78-0.92)	<0.001	**0.03***	0.37 (0.34-0.40)	0.32 (0.30-0.34)	<0.001	**0.007***
Striato-premotor Left	0.73 (0.65-0.81)	0.79 (0.65-0.93)	0.003	0.21	0.41 (0.38-0.44)	0.37 (0.33-0.42)	0.001	0.08
Striato-premotor Right	0.71 (0.67-0.75)	0.77 (0.65-0.89)	0.02	1.00	0.42 (0.40-0.44)	0.37 (0.32-0.43)	0.002	0.13
Striato-precentral Left	0.72 (0.68-0.76)	0.76 (0.66-0.86)	0.01	0.69	0.43 (0.41-0.45)	0.39 (0.37-0.41)	0.007	0.48
Striato-precentral Right	0.71 (0.68-0.74)	0.75 (0.66-0.84)	0.03	1.00	0.43 (0.42-0.44)	0.39 (0.35-0.43)	0.002	0.13
Striato-postcentral Left	0.73 (0.69-0.77)	0.77 (0.71-0.83)	0.001	0.09	0.43 (0.40-0.46)	0.40 (0.38-0.42)	0.02	1.00
Striato-postcentral Right	0.71 (0.68-0.74)	0.77 (0.71-0.83)	0.002	0.14	0.43 (0.41-0.45)	0.39 (0.36-0.42)	0.002	0.14
Striato-parietal Left	0.75 (0.72-0.78)	0.83 (0.81-0.85)	<0.001	**0.007***	0.41 (0.37-0.45)	0.37 (0.36-0.38)	<0.001	0.051
Striato-parietal Right	0.77 (0.73-0.82)	0.84 (0.79-0.89)	<0.001	**0.007***	0.40 (0.47-0.43)	0.37 (0.35-0.39)	0.001	0.09
Striato-occipital Left	0.80 (0.76-0.84)	0.92 (0.86-0.98)	0.001	0.09	0.37 (0.33-0.41)	0.34 (0.33-0.35)	<0.001	**0.01***
Striato-occipital Right	0.80 (0.76-0.84)	0.95 (0.89-1.01)	<0.001	**0.007***	0.36 (0.34-0.38)	0.331 (0.327-0.333)	<0.001	**0.01***
Brainstem								
Parieto Occipital pontine Left	0.75 (0.72-0.78)	0.80 (0.78-0.82)	<0.001	**0.01***	0.46 (0.44-0.48)	0.43 (0.41-0.45)	0.003	0.22
Parieto Occipital pontine Right	0.76 (0.72-0.80)	0.82 (0.79-0.86)	<0.001	**0.007***	0.45 (0.43-0.47)	0.41 (0.39-0.43)	<0.001	0.051
Fronto-pontine tract Left	0.74 (0.68-0.81)	0.79 (0.71-0.87)	<0.001	0.09	0.46 (0.43-0.49)	0.41 (0.38-0.44)	<0.001	**0.01***
Fronto-pontine tract Right	0.75 (0.72-0.79)	0.81 (0.75-0.87)	<0.001	**0.03***	0.45 (0.42-0.48)	0.40 (0.37-0.43)	<0.001	**0.007***
Superior cerebellar peduncle Left	0.71 (0.67-0.75)	0.77 (0.76-0.78)	0.007	0.46	0.44 (0.42-0.47)	0.42 (0.40-0.44)	0.01	0.90
Superior cerebellar peduncle Right	0.72 (0.69-0.75)	0.77 (0.75-0.80)	0.005	0.32	0.42 (0.40-0.44)	0.40 (0.37-0.43)	0.35	1.00
Inferior cerebellar peduncle Left	0.70 (0.64-0.76)	0.78 (0.77-0.79)	<0.001	**0.01***	0.40 (0.38-0.42)	0.37 (0.35-0.39)	0.03	1.00
Inferior cerebellar peduncle Right	0.70 (0.65-0.75)	0.75 (0.73-0.77)	0.005	0.32	0.38 (0.35-0.41)	0.37 (0.36-0.38)	0.15	1.00
Middle cerebellar peduncle	0.71 (0.65-0.77)	0.77 (0.75-0.79)	0.001	0.09	0.41 (0.38-0.44)	0.39 (0.37-0.41)	0.07	1.00

Table 5. Mean diffusivity and fractional anisotropy for the association fibres tracts. All data reported as median (IQR).

	Mean Diffusivity (x10⁻³ mm²/s)				Fractional Anisotropy			
	Controls	COVID-19	P-value	Adjusted P-Value	Controls	COVID-19	P-value	Adjusted P-Value
Association Fibres								
Superior longitudinal fascicle I Left	0.71 (0.68-0.74)	0.75 (0.70-0.80)	0.001	0.09	0.43 (0.40-0.46)	0.38 (0.35-0.41)	<0.001	0.051
Superior longitudinal fascicle I Right	0.72 (0.68-0.76)	0.78 (0.71-0.85)	0.001	0.09	0.43 (0.40-0.46)	0.38 (0.36-0.40)	<0.001	**0.007***
Superior longitudinal fascicle II Left	0.72 (0.68-0.76)	0.79 (0.73-0.85)	<0.001	**0.03***	0.41 (0.38-0.44)	0.35 (0.34-0.36)	<0.001	**0.007***
Superior longitudinal fascicle II Right	0.73 (0.70-0.76)	0.81 (0.73-0.89)	<0.001	**0.03***	0.40 (0.36-0.44)	0.35 (0.33-0.37)	<0.001	**0.007***
Superior longitudinal fascicle III Left	0.71 (0.67-0.75)	0.81 (0.70-0.92)	0.003	0.22	0.41 (0.38-0.44)	0.36 (0.33-0.39)	0.001	0.09
Superior longitudinal fascicle III Right	0.73 (0.69-0.77)	0.83 (0.74-0.92)	0.003	0.22	0.39 (0.36-0.42)	0.34 (0.31-0.37)	<0.001	0.051
Inferior longitudinal fascicle Left	0.77 (0.73-0.81)	0.85 (0.80-0.90)	<0.001	**0.03***	0.37 (0.34-0.40)	0.34 (0.33-0.35)	<0.001	**0.007***
Inferior longitudinal fascicle Right	0.77 (0.72-0.82)	0.89 (0.83-0.96)	<0.001	**0.007***	0.37 (0.35-0.39)	0.33 (0.32-0.34)	<0.001	**0.007***
Uncinate fascicle Left	0.76 (0.73-0.79)	0.83 (0.73-0.93)	0.001	0.08	0.38 (0.36-0.40)	0.35 (0.32-0.38)	0.06	1
Uncinate fascicle Right	0.78 (0.75-0.81)	0.88 (0.85-0.92)	<0.001	**0.02***	0.35 (0.33-0.37)	0.31 (0.30-0.32)	0.002	0.13
Arcuate fascicle Left	0.72 (0.69-0.76)	0.82 (0.75-0.89)	<0.001	**0.01***	0.38 (0.36-0.40)	0.33 (0.31-0.35)	<0.001	**0.03***
Arcuate fascicle Right	0.74 (0.70-0.78)	0.83 (0.76-0.90)	<0.001	0.051	0.38 (0.35-0.41)	0.34 (0.32-0.36)	<0.001	**0.01***
Cingulum left	0.75 (0.72-0.78)	0.84 (0.78-0.90)	<0.001	**0.01***	0.38 (0.35-0.41)	0.35 (0.34-0.36)	0.001	0.09
Cingulum right	0.74 (0.71-0.77)	0.84 (0.78-0.90)	<0.001	**0.007***	0.38 (0.33-0.43)	0.34 (0.32-0.36)	<0.001	**0.01***
Middle longitudinal fascicle Left	0.76 (0.73-0.79)	0.84 (0.80-0.89)	<0.001	**0.007***	0.37 (0.34-0.40)	0.33 (0.32-0.34)	<0.001	0.051
Middle longitudinal fascicle Right	0.77 (0.72-0.82)	0.85 (0.80-0.90)	<0.001	**0.007***	0.37 (0.34-0.41)	0.34 (0.32-0.34)	<0.001	0.051
Inferior occipito-frontal fascicle Left	0.80 (0.76-0.84)	0.92 (0.87-0.97)	<0.001	**0.01***	0.35 (0.33-0.37)	0.32 (0.31-0.33)	0.002	0.14
Inferior occipito-frontal fascicle Right	0.81 (0.77-0.85)	0.96 (0.88-1.04)	<0.001	**0.007***	0.33 (0.31-0.35)	0.29 (0.28-0.30)	<0.001	0.051
Optic Radiation Left	0.81 (0.78-0.84)	0.90 (0.84-0.96)	0.001	0.09	0.37 (0.34-0.40)	0.34 (0.33-0.35)	<0.001	0.051
Optic Radiation Right	0.80 (0.77-0.83)	0.92 (0.87-0.97)	<0.001	**0.007***	0.39 (0.37-0.41)	0.34 (0.32-0.36)	<0.001	**0.007***

Acknowledgements and Funding

Supplementary References

1.   Ledig C, Heckemann RA, Hammers A, et al. Robust whole-brain segmentation: application to traumatic brain injury. *Med Image Anal* 2015; **21**(1): 40-58.

2.   Manjon JV, Coupe P, Concha L, Buades A, Collins DL, Robles M. Diffusion weighted image denoising using overcomplete local PCA. *PLoS One* 2013; **8**(9): e73021.

3.   Veraart J, Novikov DS, Christiaens D, Ades-Aron B, Sijbers J, Fieremans E. Denoising of diffusion MRI using random matrix theory. *Neuroimage* 2016; **142**: 394-406.

4.   Veraart J, Fieremans E, Jelescu IO, Knoll F, Novikov DS. Gibbs ringing in diffusion MRI. *Magn Reson Med* 2016; **76**(1): 301-14.

5.   Jeurissen B, Tournier JD, Dhollander T, Connelly A, Sijbers J. Multi-tissue constrained spherical deconvolution for improved analysis of multi-shell diffusion MRI data. *Neuroimage* 2014; **103**: 411-26.

6.   Andersson JLR, Sotiropoulos SN. An integrated approach to correction for off-resonance effects and subject movement in diffusion MR imaging. *Neuroimage* 2016; **125**: 1063-78.

7.   Wasserthal J, Neher P, Maier-Hein KH. TractSeg - Fast and accurate white matter tract segmentation. *Neuroimage* 2018; **183**: 239-53.

8.   Friston KJ, Rotshtein P, Geng JJ, Sterzer P, Henson RN. A critique of functional localisers. *Neuroimage* 2006; **30**(4): 1077-87.

9.   Maldjian JA, Laurienti PJ, Kraft RA, Burdette JH. An automated method for neuroanatomic and cytoarchitectonic atlas-based interrogation of fMRI data sets. *Neuroimage* 2003; **19**(3): 1233-9.

10.   Edlow BL, Takahashi E, Wu O, et al. Neuroanatomic connectivity of the human ascending arousal system critical to consciousness and its disorders. *J Neuropathol Exp Neurol* 2012; **71**(6): 531-46.

11.   Avery MC, Krichmar JL. Neuromodulatory Systems and Their Interactions: A Review of Models, Theories, and Experiments. *Front Neural Circuits* 2017; **11**: 108.

12.   Newcombe VFJ, Das T, Cross JJ. Diffusion imaging in neurological disease. Journal of Neurology 2013;**260**:335-342.